MARTINI coarse-grained model for poly--caprolactone in acetone-water mixtures

MARTINI Coarse-Grained Model for Poly-ε-Caprolactone in Acetone-Water Mixtures

Alessio D. Lavino[1*§], Paola Carbone[2] and Daniele Marchisio[1]

[1] *Department of Applied Science and Technology, Politecnico di Torino, Torino, Italy;*
[2]*School of Chemical Engineering & Analytical Science, The University of Manchester, Manchester, United Kingdom*

*corresponding author: Department of Applied Science and Technology, Institute of Chemical Engineering, Politecnico di Torino, 10129 Torino, Italy. E-mail: alessio.lavino@polito.it

ABSTRACT

In this work we present the development of a MARTINI-type coarse-graining (CG) model for poly-ε-caprolactone (PCL) dissolved in a solvent binary mixture of acetone and water. A thermodynamic/conformational procedure is adopted to build up the CG model of the system, starting from the standard MARTINI force field. The single CG bead is parametrised upon solvation free energy calculations, whereas the conformation of the whole polymer chain is optimized using the radius of gyration values calculated at different chain lengths. The model is then able to reproduce the correct thermodynamics of the system, as well as the conformation of single PCL chains, especially in pure water and acetone. The results obtained here are then used to simulate the interactions between multiple longer PCL chains in solution. The model here developed can be promisingly used in the future to achieve a deeper insight into the dynamics of the polymer self-assembly.

KEYWORDS

binary mixtures, MARTINI, molecular dynamics, nanoparticles, self-assembly.

1 INTRODUCTION

In the recent decades, molecular simulations have become a pivotal tool for understanding the complexity of the key phenomena involved in many areas of physics, [1,2] engineering and applied science[3-5] (biological systems,[6] soft matter,[7] colloids). One of the most used molecular simulation tools is represented by molecular dynamics (MD).[8] Due to the large time and length scales involved in many biological and soft matter applications, the solely atomistic MD turns out to be insufficient to fulfil a complete insight into such complex systems. Coarse-grained molecular dynamics (CGMD) is then needed, in order to reduce the number of degrees of freedom (DOF),[9-12] by grouping a given number of atoms together in a unique particle denominated "bead". Thanks to the possibility of simulating larger systems for very long times, CGMD is becoming more and more popular in the investigation of many biological and complex systems, such as proteins,[13] DNA[14] and lipids.[15]

Different classifications may be done among the several existing CG techniques; basically, it is possible to identify two main categories: the bottom-up and the top-down CG models. The latter are built up upon experimental data observed at the length scale at which the CG model is targeted to. The former are systematically derived from first principles or atomistic detailed-level MD. Examples of bottom-up CG models are the Iterative Boltzmann Inversion (IBI), [16] the Inverse Monte Carlo[17] (this one by means of Monte Carlo

simulations), the force-matching models[18-20] and more rigorous derived[21] bottom-up techniques such as the conditional reversible work (CRW),[22] which uses thermodynamic cycles to calculate non-bonded interaction potentials and the Mori-Zwanzig framework,[23,24] capable of deriving a closed set of equations for the dynamics of CG systems.

At higher coarse-graining levels of resolution, mesoscopic CG models have been developed in order to capture the system hydrodynamics, such as the multiparticle collision dynamics[25] and the well-known dissipative particle dynamics (DPD).[26] Developed at the beginning as a top-down model, recent works showed that bottom-up approaches may be used in order to achieve more accurate information about the range of validity of the DPD assumptions (especially concerning the Markovian friction term).[27] Furthermore, DPD can be systematically derived via bottom-up techniques, such as the CRW-DPD.[28] It is worth noticing also that the rigorous Mori-Zwanzig derivation can lead to the mathematical framework of DPD, despite the two approaches are completely different. Interesting applications of DPD on co-polymer systems have been recently done, by studying their rheological behaviour in water solutions.[29,30]

Other CG methods can be built up as a combination of both top-down and bottom-up techniques. This is the case of the MARTINI force field, developed by Marrink et al[31] Optimized at the beginning only for lipids systems,[15] it has been extended throughout the years to other biological systems, such as proteins,[32] carbohydrates,[33] DNA[34] and also employed to model polymer melts and solutions.[35] MARTINI CG bead types have been parametrized by reproducing the partitioning free energies between polar and apolar phases of a large number of chemical compounds. Despite the MARTINI CG force field is able to catch the partition properties of several compounds in different mixtures, recent works by Rossi,[36] Lee,[37] Lee and Larson[38], Taddese and Carbone[39] and Milani[40] have shown how the MARTINI force field can be suitably adjusted and improved for polymer systems, introducing new bead types compatible with the existing ones. These new beads can be parametrised through the tuning of several properties, such as the solvation free energy. Polymer systems still represent a challenging area, because of the several properties concerning the polymer chain lengths, as well as the different conformations they assume depending on the environment. More specifically, polymer self-assembly in solution (of particular interest due to numerous applications[41,42,43]) is still a challenge from a simulation point of view due to the subtle effects that solvents and temperature have on the polymer conformation. Particularly important is the understanding of the polymer chain behaviour in

"good" and "bad" solvents and a mixture of them.

Here, the case of poly-ε-caprolactone (PCL) in acetone-water mixtures is studied, due to its impact on numerous applications such as controlled drug delivery systems, in which the control of the targeted size and the particle size distribution is of paramount importance.[44] PCL represents one of the most suitable candidates in nanoparticles drug delivery, thanks to its biocompatibility, as its biodegradation products are non-toxic for human health.[45] PCL nanoparticles can be loaded with specific drugs and, as molecular carriers, they represent nowadays a valid alternative to the more aggressive cancer treatments, overcoming all the very well-known side effects.[46-48] The controlled release in targeted delivery systems is extremely sensitive to the mean size of the nanoparticles (nanocarriers), in turn, dependent on the way in which the polymer nanoparticles are produced. One of the most used techniques is the so-called flash nano-precipitation (FNP), a solvent displacement process based on the extremely fast mixing of "good" and "bad" solvents.[49] In FNP, the solute (e.g., PCL) is initially dissolved in a "good" solvent stream (e.g., acetone). The "good" solvent is rapidly mixed with a "bad" solvent flow (e.g., water); the role played by the "bad" solvent (or anti-, or non-solvent) is to destabilise the mixture, inducing polymer aggregation, nanoparticles formation, and, consequently, precipitation. This spontaneous aggregation is sometimes referred to as "self-assembly",[44,49] as it will labelled from now on throughout the whole manuscript. Due to the several phenomena involved, spanning different length scales, further insights at the molecular level must be reached and taken into account.

Hence, the aim of this work is to develop and validate a CG model for the PCL in solution, based on the MARTINI CG force field and suitably modified to account for the thermodynamics of a mixed system containing polymers chains and two solvents in different concentrations. The parameter space optimized by using the standard "MARTINI approach" is expanded including solvation free energies of the monomer (calculated by means of the Bennett's Acceptance Ratio method[50]), and the conformation of the polymer chains in terms of radius of gyration. The validation of the model has been done by comparing it against the atomistic simulations, some of which are performed in this work, others in a previous one.[51] Once all the parameters related to a single CG polymer chain are set up, it is possible to use this CGMD model to simulate larger systems and systems involving multiple polymer chains in the simulation box.

The paper is structured as follows: section 2 is dedicated to the atomistic simulations,

with particular attention to the well-known de-mixing problems of acetone-water mixtures; section 3 deals with the CG model of PCL in solution; section 4 gives a deeper insight into the thermodynamic method used for the solvation free energy calculations; simulation protocols (for both atomistic and CG) are presented in section 5; results and discussions are shown in section 6; conclusions and future developments remarks are reported in section 7.

2 ATOMISTIC SIMULATIONS OF ACETONE-WATER MIXTURES

Despite water and acetone are completely miscible at room temperature, it is well-known that acetone-water mixtures undergo unphysical de-mixing in all-atom MD simulations,[52] especially in a specific acetone molar fractions range (x_A= 0.10 ÷ 0.50). The de-mixing has been shown[53] to be caused by the high hydrophobicity of acetone atomistic force fields, not being able to be polarized by high-water concentration environments (induced-polarization). Pereyra et al[52] showed that it is possible to overcome the phase separation by increasing the polarization of the mixture, more specifically, by changing the charge distribution of the acetone molecule. Following this approach, different charge distributions (depending on mixture molar fraction) on the acetone molecule have been used in our simulations as shown in Table 1. Polarization is strictly related to the dipole moment of a molecule, being defined as the charge displacement multiplied by the intensity of the charge being displaced.[54] Due to the symmetry of the acetone molecule, the more the charges are displaced, or, equally, the higher is the module of the charge value on the carbonyl axis, the higher is the dipole moment and, consequently, the higher is the polarizability of the molecule. The charge distributions adopted in this context lead to an acetone dipole moment sufficiently high (Table 1) to guarantee a good affinity with the water model, therefore no de-mixing occurs during the MD simulations. An alternative approach to increase the polarizability of acetone in water-rich environments consists in implementing a charge-on-particle (COP) model on the carbonyl group, which has the advantage to keep the charge distribution constant with the mixture composition. Further details on COP model can be found in Lavino et al[55] Here, the charge distribution approach has been adopted as shown in Table 1, in which C2-O2 corresponds to the acetone carbonyl group.

Table 1. Acetone charge (e) distribution used at different acetone molar fractions, x_A. C2-O2 corresponds to the carbonyl group; carbons (C) and hydrogens (H) refer to the two methyl

groups of the acetone molecule. For each charge distribution, the corresponding acetone dipole moment is reported.

x_A	C2	O2	C (methyl)	H (methyl)	Dipole Moment, *D*
0.25	0.79	-0.73	-0.36	0.11	4.60
0.50	0.79	-0.73	-0.36	0.11	4.60
0.75	0.55	-0.55	-0.27	0.09	3.69
1.00	0.47	-0.47	-0.18	0.06	3.07

In the atomistic simulations, the OPLS/AA force field was used to model the solute molecules, whereas the TIP4P model was used for water. The data reported in the last row in Table 1 corresponds to the original charges of the OPLS/AA force field. Those have been used to model the pure acetone system, while a properly modified set of charges were used at the other acetone molar fractions, in order to avoid phase separation. Using the charge distributions reported in Table 1 no de-mixing takes place, as qualitatively shown in Figure 1.

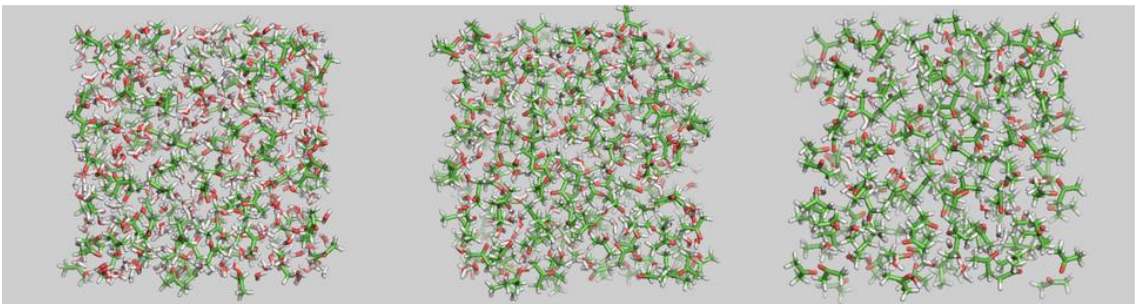

Figure 1. From left to right there are reported the three snapshots related to acetone molar fractions equal to 0.25, 0.50 and 0.75 respectively in cubic simulation boxes of 3 nm length. It is clear how no de-mixing occurs.

From a more quantitative point of view, in order to detect possible de-mixing behaviours, it is noteworthy to evaluate also the radial distribution functions (RDF), $g_{\alpha\beta}$. Figure 2 (top panel) shows the acetone-acetone RDF, g_{AA} (r), and it is clear that acetone clustering is not detected at all acetone molar fractions, since no first peak is observed. Results are in line with those obtained by Lavino et al[55] in which clustering effect vanishes at all acetone molar fractions, thanks to a pseudo-polarizable model. It is then possible to infer that under these operating conditions the system can be considered well micro-mixed enough to perform all the sets of atomistic simulations which the single CG beads will be characterised on. All the atomistic details concerning the latter point will be accurately presented in subsection 5.1.

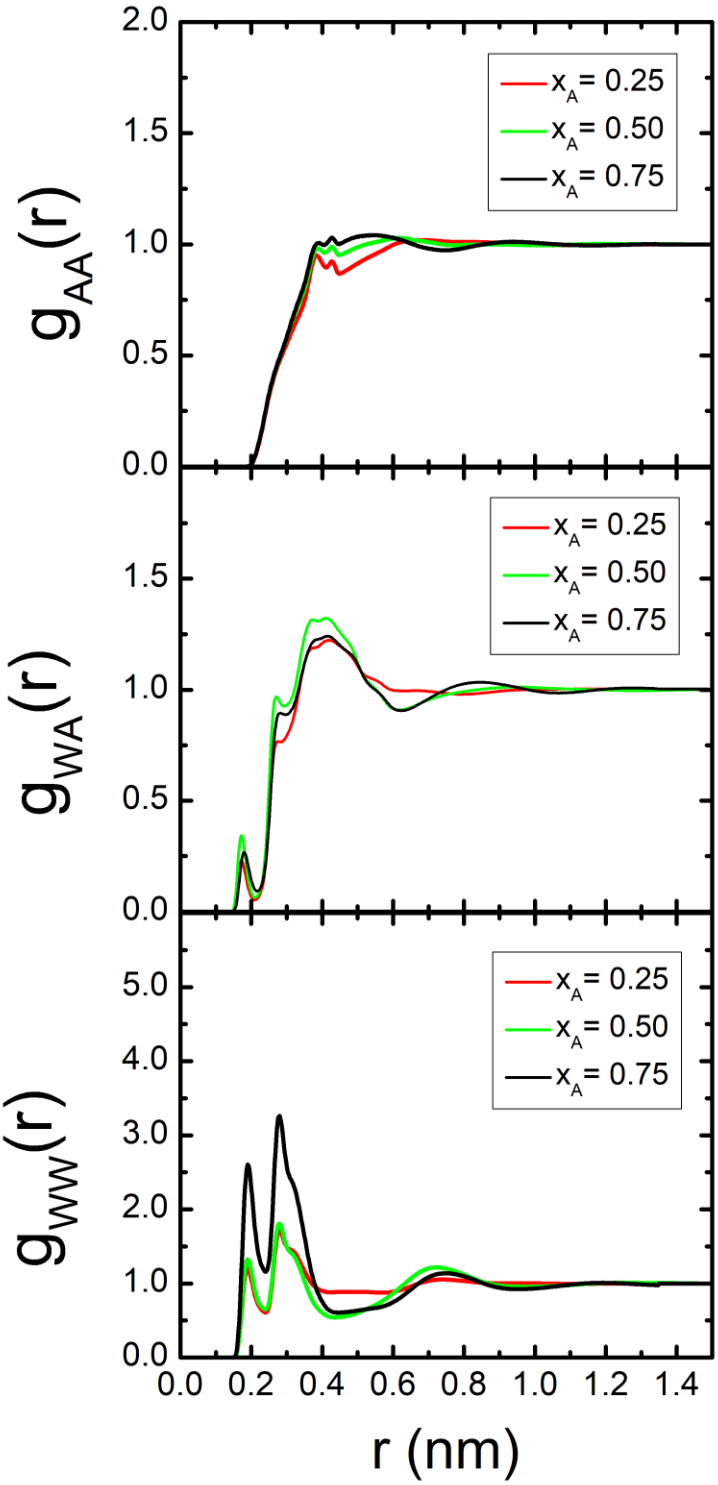

Figure 2. Atomistic radial distribution functions for acetone-acetone, $g_{AA}(r)$, water-acetone, $g_{WA}(r)$ and water-water, $g_{WW}(r)$, at different acetone molar fractions, x_A, in function of the generic distance r. The red, green and black lines correspond respectively to x_A= 0.25, 0.50 and 0.75.

3 COARSE-GRAINED MARTINI MODEL

In line with the MARTINI force field,[31] a 4:1 mapping has been considered, which means four heavy atoms per CG bead. The two beads of the PCL repeat unit have been chosen in order to account for both the alkyl and the ester part of the polymer, starting from existing bead types tabulated in the MARTINI force field. Therefore, at the beginning a C_1 bead type (corresponding to butane) was used for the alkyl part, whereas a bead type labelled N_{am} (corresponding to methyl formate) was used for the ester part, based on the existing one N_a and suitably modified in order to differentiate it from N_a, which corresponds to acetone. Water is modelled by a P_4 bead type (corresponding to four water molecules), in line with the MARTINI force field. The mapping of the system is schematically depicted in Figure 3. It is crucial to stress that this mapping (N_{am} - C_1) represents just a starting choice, since the outcome of the CG optimization procedure we adopt here may lead to different bead types (for more suitably describing the behaviour of PCL in acetone/water mixtures) as it will be shown in the results section.

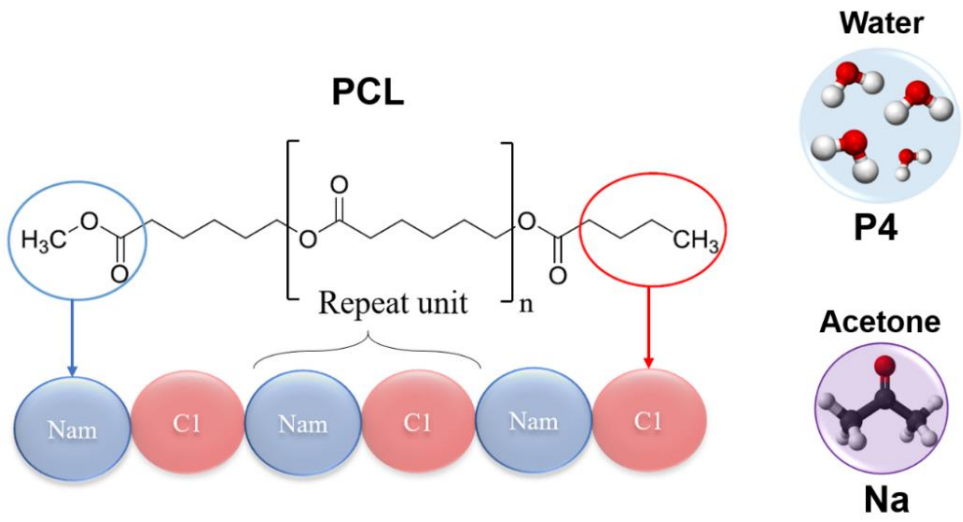

Figure 3. Initial mapping of both the PCL chain and the solvents used in this work. The repeat unit is described by N_{am} and C_1 bead types respectively for the ester and the alkyl part. These choices represent just a starting point for the optimization procedure in building up the CG model. Water and acetone are instead mapped respectively by P_4 and N_a bead types.

The approach proposed here consists in parametrising the conservative potentials of the single CG beads by matching the atomistic results in terms of solvation free energy, evaluated by using the BAR method[50] (explained in the next section). More specifically, the Lennard-Jones (LJ) parameter ε has been varied, keeping σ constant. The default MARTINI non-bonded LJ interaction levels have been used to build up the model, in line with the MARTINI force field.

Every interaction between bead types is biunique as reported in the interaction matrix of the MARTINI work.[31] A pairwise LJ 12-6 potential energy function:

$$V_{LJ}(r) = 4\varepsilon_{ij}\left[\left(\frac{\sigma_{ij}}{r}\right)^{12} - \left(\frac{\sigma_{ij}}{r}\right)^{6}\right], \quad (1)$$

is used to describe non-bonded interactions between CG beads, where σ_{ij} represents the closest distance between two particles and ε_{ij} the strength of their interaction. Since CG beads have no net charge in the present system, then no Coulombic interaction is explicitly accounted for.

Concerning the bonded interactions, weak harmonic potentials have been used for both bonds and angles:

$$V_b(R) = \frac{1}{2}K_b(r - r_b)^2 \quad (2)$$

$$V_{angle}(\theta) = \frac{1}{2}K_{angle}(\theta - \theta_0)^2, \quad (3)$$

where $K_b$and r_b are respectively the bond stretching force constant and the equilibrium bond length, while K_{angle} and θ_0 are respectively the angle force constant and the equilibrium angle. Their values will be reported in the simulation details section.

4 BENNETT'S ACCEPTANCE RATIO METHOD

The free energy of solvation , ΔG^{solv}, is evaluated by means of the Bennett's Acceptance Ratio (BAR) method,[50] since it has been shown that it represents a more efficient method compared to other thermodynamic integration methods.[56,57] It is evaluated as the balance between the work required for the production of a cavity in the bulk solvent, plus the gain reached to solvate a given solute which gradually compares in that cavity and

interacts with the surrounding solvent molecules, in terms of Van der Waals, Coulomb and hydrogen interactions. Although the work related to the cavity production is always an unfavourable process, the gain in terms of enthalpic and entropic solvation can be more or less favourable, depending on the solute hydrophobicity (if the solvent is pure water) or, in general, on the affinity with the solvent. ΔG^{solv} can be interpreted as the balance between these two factors.[58-60]

From a computational point of view, the BAR method is based on a switching/interacting parameter, λ, which states the coupling between the solute and the solvent, and spans the range [0,1]. At λ=0 (non-interacting state) a cavity is created in the bulk solvent (vacuum); on the other hand, λ=1 stands for a fully interacting state between the solute and the solvent. All the other values in between [0,1] represent a gradual appearance of the solute in the cavity. The chosen number of λ points represents a crucial aspect of this method, being a trade-off between computational costs and phase-space overlap[61] along the thermodynamic pathway. The total ΔG^{solv} can be expressed as

$$\Delta G^{solv} = \sum_{i=1}^{N} \Delta G_i^{BAR}(\lambda_{i-1}, \lambda_i), \tag{4}$$

where $\Delta G_i^{BAR}(\lambda_{i-1}, \lambda_i)$ is the ΔG^{solv} related to the single interval $[\lambda_{i-1}, \lambda_i]$, evaluated by means of the BAR method on the *N* intervals.

Computational details about ΔG^{solv} calculations will be reported in the next section; potential functions deserve particular attention. More specifically, soft-core potentials have been used for the BAR simulations, to avoid singularities when non-bonded interactions are turned off. Soft-core potentials V_{sc} are defined as a shifted version of the regular potentials:

$$V_{sc}(r) = (1-\lambda)V_A(r_A) + \lambda V_B(r_B), \tag{5}$$

$$r_A = (\alpha\sigma_A^6\lambda^p + r^6)^{1/6}, \tag{6}$$

$$r_B = (\alpha\sigma_B^6(1-\lambda)^p + r^6)^{1/6}, \tag{7}$$

where $V_A(r_A)$ and $V_B(r_B)$ are the normal "hard-core" potentials referred to the states *A* and *B*, α is the soft-core parameter (it controls the value of the potentials when r is approaching to zero), p is the soft-core λ power and σ is the radius of the interaction.

5 SIMULATION DETAILS

All simulations were performed by using GROMACS 4.5.6 molecular dynamics package.[62] VMD program was used to produce graphical images of the investigated molecular systems.

5.1 Atomistic simulations

The atomistic simulations were carried out in a cubic box with periodic boundary conditions and box length equal to 3 nm, in an NPT ensemble. The OPLS-AA force-fields was employed for acetone (suitably modified according to the charge distributions shown in section 2) and TIP4P force field for water. The weak harmonic potential functions were used for bonds, angles and improper dihedrals, whereas the Ryckaert-Bellemans potential was implemented for the proper dihedrals. A single butane and a single methyl formate (corresponding to the atomistic part of the single CG beads) molecule were simulated in acetone-water mixtures at acetone molar fractions equal to 0, 0.25, 0.50, 0.75, 1. The energy minimization of the system was carried out with a steepest descent algorithm. The system was then equilibrated by using a leap-frog algorithm for 1 ns with a 2 fs timestep. Berendsen thermostat and Berendsen barostat (coupled with Parrinello-Rahman) fixed the temperature and the pressure respectively at 300 K and 1 bar during the equilibration, with a coupling time constant respectively equal to 0.2 ps and 5 ps. Simulations were performed for 10 ns with a 1 fs timestep and bonds were constrained using the LINCS algorithm. Three-dimensional periodic boundary conditions were employed and electrostatic interactions were evaluated using the Particle-mesh Ewald (PME) summation. A temperature of 300 K was maintained by means of a velocity-rescale algorithm with a time constant equal to 0.1 ps. An isotropic pressure of 1 bar was set by using a Parrinello-Rahman scheme with a coupling constant equal 1.0 ps and a compressibility set to 4.5 10^{-5} bar^{-1}. The cutoff radius of the non-bonded interactions was set to 0.9 nm. To keep away from singularities and numerical instabilities, a soft-core LJ and Coulomb potentials were used[63] in the thermodynamic simulations with the BAR method, as reported in section 4. A stochastic dynamics integrator was implemented in order to avoid singularities when λ approaches to zero and the number of lambda points has been chosen equal to 10 for the butane and 20 for the methyl formate, in line with the theory reported in section 4. Concerning the soft-core potential parameters reported in Equations (5-7) and used in the atomistic BAR simulations, p was set equal to 1, α equal to 1 and σ equal to 0.3 nm.

5.2 Coarse-grained simulations

The CG simulations were performed in a cubic box, whose length varied depending on the simulated system. It spans from 4 nm for the simulation of the single CG bead in mixture to 15 nm for the longest PCL chains. Different PCL chains lengths have been simulated. In particular, we initially focused on PCL-10, PCL-20 and PCL-30, namely a PCL chain with a number of repeat units respectively equal to 10, 20 and 30, for the CG model validation. Longer PCL chains have also been considered up to 60 repeat units. A shifted function for the non-bonded interactions has been applied to Equation (1) between the inner and outer cutoff radii respectively equal to 0.9 and 1.2 nm. The parameters for the bonded potentials, reported in Equations (2) and (3), are $r_b = 0.415$ nm, $\theta_0 = 170°$ (P_2-C_α-P_2) $\theta_0 = 129°$ (C_α-P_2-C_α) and the force constants $K_b = 5000$ kJ mol^{-1}nm^{-2} and $K_\theta = 50$ kJ mol^{-1}, since it was already demonstrated that this set of values can correctly reproduce the atomistic distributions.[64]

The energy minimization was carried out by means of the steepest descent algorithm. The system was equilibrated with a leap-frog algorithm for 1-2 ns by using a Berendsen thermostat and a combination of Berendsen and Parrinello-Rahman barostat (T = 300 K and p = 1 bar). The temperature time constant for the Berendsen scheme is equal to 1 ps, Parrinello-Rahman coupling time constant is equal to 4-12 ps (higher constants values ensure more stability). The simulations were performed for 50 ns with a 20 fs timestep. A velocity-rescale thermostat scheme was used with a temperature time constant of 1.0 ps, whereas a Parrinello-Rahman barostat was employed with a time constant equal to 4 ps and a compressibility set to 4.5 10^{-5} bar^{-1}. A soft-core LJ and Coulomb potentials were used for BAR calculations, and the number of lambda points has been chosen equal to 10 for both of the CG solutes. Concerning the soft-core potential parameters reported in Equations (5-7) used in the CG BAR simulations, the soft-core parameters have been chosen to be p equal to 1, α equal to 0.5 and σ equal to 0.47 nm.

6 RESULTS AND DISCUSSION

In this section, the main results about the developed CG model and the adopted methodology will be discussed. First of all, it is noteworthy to underline that, unlike the atomistic system, CG acetone-water mixtures do not lead to evident phase separation or de-mixing. Little clusters seem to appear, as shown in Figure 4a and 4b, in which a snapshot of the simulation

box of N_a-P_4 (CG acetone-water) mixture at $x_A = 0.25$ and box length equal to 15 nm, with 27000 particles and after 10 ns is reported. Since the system does not undergo an evident phase separation, by looking at the snapshots reported in Figure 4, it is reasonable to infer that no de-mixing occurs at the CG level. This is also confirmed from a more quantitative analysis by looking at the density profiles along the three spatial directions *x, y, z* (Figure 4c, d, e) that appear to be flat. Since the de-mixing observed with the atomistic force field is caused by the inability of the model to reproduce the polarization response of acetone molecule in water,[55] the reason why this does not take place with the CG model, is due to the fact that the CG beads do not carry any explicit charge.

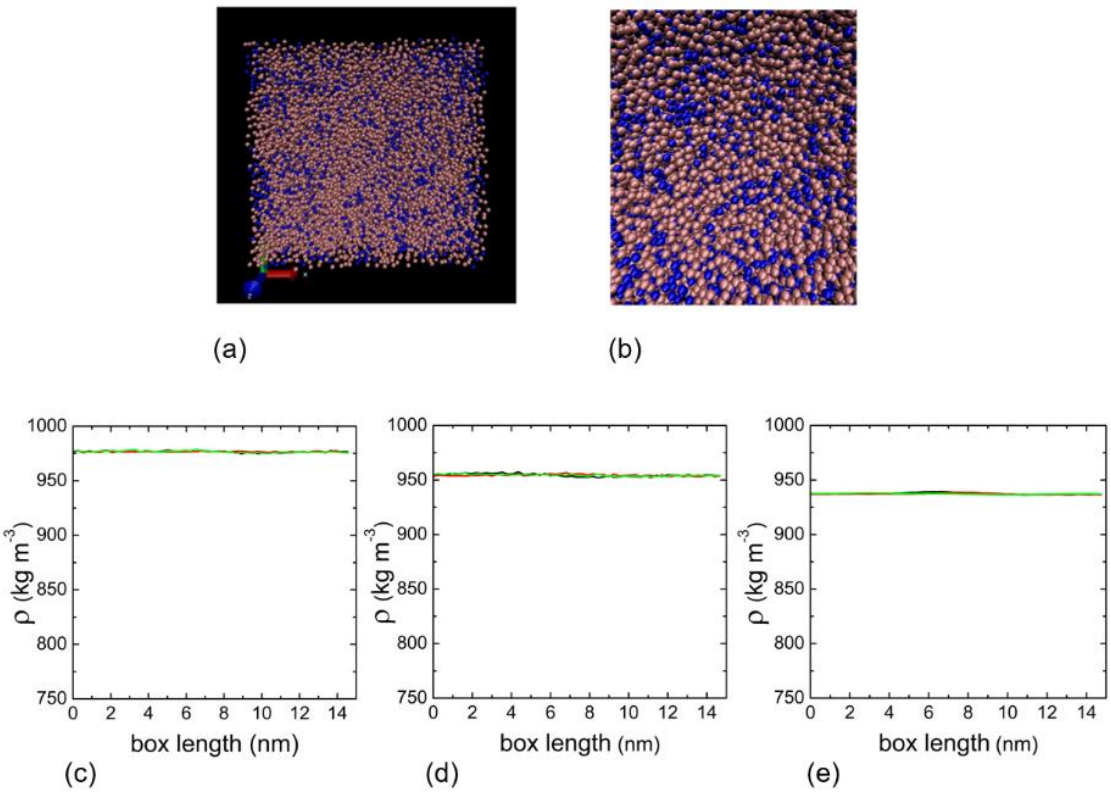

Figure 4. (a) Snapshot of the N_a-P_4 CG acetone(blue)-water(pink) mixture for $x_A = 0.25$ and box length equal to 15 nm, with 27000 particles and after 10 ns. (b) Detail of the N_a-P_4 box in which a little cluster (blue, N_a) it seems to form; however, no evident phase separation is detected at the CG level. Densities profiles along x (black), y (red) and z (green) are reported at acetone molar fraction equal to 0.25 (c), 0.50 (d) and 0.75 (e).

6.1 Estimation of the solvation free energy of a single bead

Firstly, atomistic and CG simulations of a single bead in solution were carried out, in order to match the ΔG^{solv} between the CG beads and the atomistic part of the polymer chain that it represents (mapping). Therefore, atomistic models for butane, methyl formate, and the beads C_1 and N_{am} are simulated in acetone-water mixtures and the relative ΔG^{solv} are evaluated. The main results are shown in Figure 5.

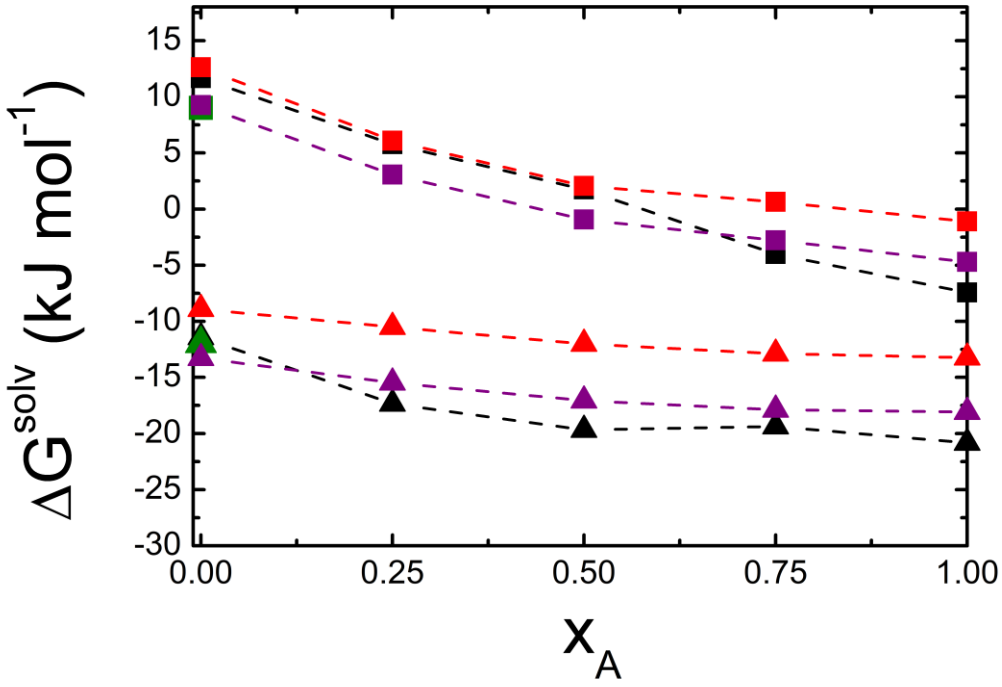

Figure 5. Free energy of solvation of butane (squares) and methyl formate (triangles) in mixture from the atomistic simulations (black symbols) carried out in this work. The red symbols refer to the MARTINI model, C_1 (squares) and N_{am} (triangles), without any modifications of the LJ parameter, ε. The purple symbols refer to the CG model developed here, in terms of single beads (squares for the alkyl part and triangles for the ester part of the PCL repeat unit) varying suitably the LJ parameter, ε. The green symbols stand for the experimental ΔG^{solv} values respectively of butane and methyl formate in pure water.

Figure 5 clearly points out that the MARTINI beads C_1 and N_{am} (red symbols) show a mismatch with the atomistic results, in terms of ΔG^{solv} for the whole composition of the mixture. The mismatch is quite evident at high acetone molar fractions, as far as the butane is

concerned, and for the whole acetone molar fraction range, for the methyl formate. By properly modifying the LJ parameter ε, namely, by moving upwards and downwards along the MARTINI LJ interaction levels, a better agreement in terms of ΔG^{solv} between atomistic and CG model is here achieved (purple profiles in Figure 5). The only experimental values available in the literature are those referred to pure water.[65] It is evident that the agreement between atomistic, experimental and CG values is improved also in pure water (Figure 5, x_A=0).

The new set of LJ parameters (between CG solvents and CG polymer bead types) that best fit the ΔG^{solv} (purple profiles in Figure 5) is reported in Table 2. By looking at Table 2, it is worthwhile to stress that the hydrophilicity of the ester part of the PCL is enhanced in acetone-water mixtures, behaving at the CG level of resolution as a P_2 bead type (polar), instead of an N bead type (non-polar) as considered in the initial mapping. This implies that, in order to better reproduce the atomistic and experimental ΔG^{solv} in acetone-water mixtures, a more polar bead type is necessary to suitably describe the affinity of such a group in a mixture of solvents with which polarizable effects may take place. This can be justified by looking at the atomistic scale, in which water can create hydrogen bonds with the carboxyl group of the PCL. In a CG framework, hydrogen bonds and polarization effects are lost (due to the CG procedure) since groups of atoms are enclosed in the same entity, i.e. "bead", and this more favourable interaction can be taken into account by increasing the interaction strength between the polymer bead and the solvents from a MARTINI type-III (ε = 4.0 kJ/mol) to a type-II (ε = 4.5 kJ/mol). Therefore, in the mapping procedure, the bead N_{am} is substituted by a P_2 bead type.

Concerning instead the alkyl part of the PCL repeat unit, it is clear, by looking at Figure 5, that the original choice of the MARTINI-bead (C_1) overestimates the experimental (green symbol) ΔG^{solv} in pure water. In order to better reproduce the experimental value, the bead needs to be again more polar (higher values of ε). However, in this case, the choice of the correct bead type is complicated by the fact that in the current MARTINI matrix, there is no bead that is capable of reproducing the thermodynamics of butane with water (P_4 bead), acetone (N_a bead) and its mixtures. Our solution is to create a new hybrid bead, C_α, which still belongs to the range of the non-polar C bead types family of the MARTINI force field but interacts at different level with the two solvent beads. The interactions types that best fit the atomistic thermodynamics data, together with the original MARTINI ones, are reported in Table 2.

Table 2. Lennard-Jones interactions MARTINI levels and corresponding ε parameter values, between the repeat unit bead types P_2, C_α and the solvent bead types P_4 and N_a. The original MARTINI bead types, employed at the beginning of the model development, are also reported.

		POLYMER REPEAT UNIT							
		N_{am}		C_1		P_2		C_α	
		LJ interaction level	ε (kJ mol^{-1})	LJ interaction level	ε (kJ mol^{-1})	LJ interaction level	ε (kJ mol^{-1})	LJ interaction level	ε (kJ mol^{-1})
SOLVENT	P_4	III	4.0	VIII	2.0	II	4.5	VII	2.3
	N_a	III	4.0	VI	2.7	II	4.5	V	3.1

6.2 Conformational investigation of the polymer chain

Once the "polymer single bead – solvent" non-bonded interactions are optimized upon the mixture thermodynamics, an investigation on the polymer chain conformational properties can be carried out. The aim here is to suitably adjust the PCL intrachain LJ parameter ε, in order to get the best accordance with the polymer atomistic radii of gyration. Three different PCL chain lengths are used here to develop the CG model: PCL-10 (ie, 10 monomers), PCL-20 (20 monomers) and PCL-30 (30 monomers), being these the only ones investigated in the literature at the atomistic level, at all the acetone mixture fractions, in a previous work.[51] Being the conformation of the PCL chains very sensitive to intrachain non-bonded modifications, a non-trivial trade-off analysis must be carried out in order to correctly reproduce the atomistic results for PCL-10, PCL-20 and PCL-30. After this has been done, by using this set of LJ parameters, higher molecular weights are investigated (PCL-40 and PCL-60), as well as the self-assembly

in the two pure solvents and reported at the end of this work. This trade-off procedure starts from the default MARTINI non-bonded intrachain parameters that, however, were shown in a previous attempt[64] to lead to unphysical trends of the radius of gyration (it decreases at increasing chain lengths) at medium acetone molar fraction. For this reason, they represent a starting point and, consequently, suitable modifications need to be done.

At the end of the optimization procedure, the best fitting (in terms of accordance with atomistic radii of gyration among PCL-10, PCL-20 and PCL-30) is represented by the LJ intrachain interaction levels of type II (ε = 4.5 kJ/mol) for the intrachain interaction P_2- P_2, III (ε = 4.0 kJ/mol) for C_α- C_α and IV (ε = 3.5 kJ/mol) for P_2- C_α. The results are schematically shown in the Table 3 and depicted in Figure 6. Also higher molecular weights (PCL-40 and -60) are investigated with the CG model and the corresponding mean radii of gyration are reported in Table 3. As it can be seen, the agreement is very good in pure water and at high acetone molar fractions. However, the agreement is still acceptable but deteriorates at intermediate acetone molar fractions in the mixture (eg, x_A=0.50). Let us stress here that despite the intrachain P_2-P_2 and P_2-C_α interactions are in accordance with those tabulated in the MARTINI force field, the optimal C_α-C_α LJ interaction level turns out to be one level stronger (level III, ε = 4.0 kJ/mol) than the ones (level IV, ε = 3.5 kJ/mol) reported in the interaction matrix of the MARTINI force field. This stresses again what was already pointed out for the single-bead characterization: in order to capture more chemical/conformational details of the atomistic systems, the corresponding CG framework with the MARTINI force field would need more LJ interaction levels, namely, a finer discretization of them.

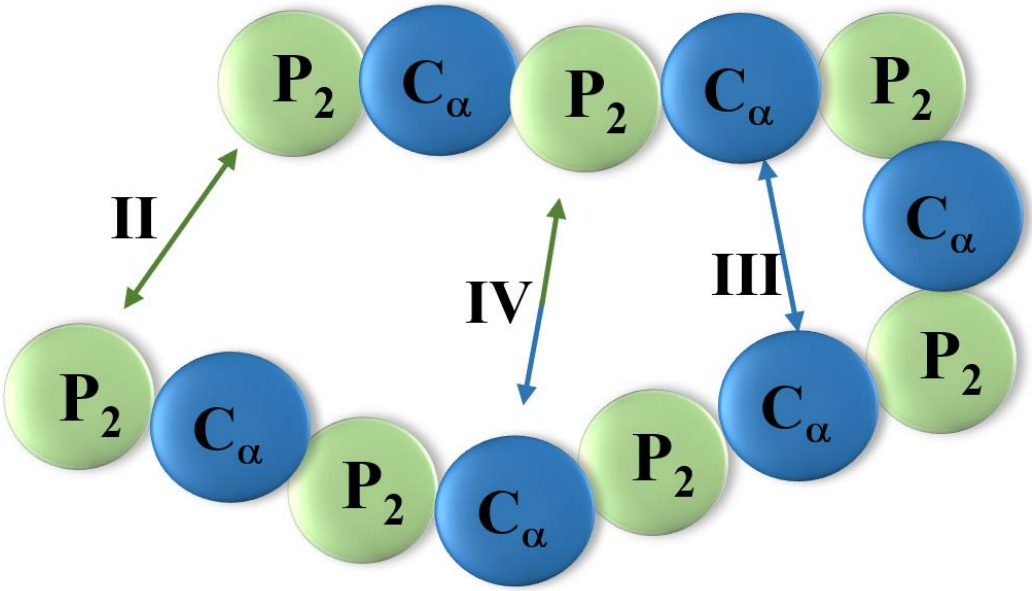

Figure 6. Snapshots referred to the final configuration of the CG PCL, after the optimization procedure conducted on the atomistic radius of gyration. The LJ interaction levels are: II (ε = 4.5 kJ/mol) for the intrachain interaction P_2- P_2, III (ε = 4.0 kJ/mol) for C_α- C_α and IV (ε = 3.5 kJ/mol) for P_2- C_α. This scheme refers to the numerical results reported in Table 3.

Table 3. Mean radius of gyration, $\langle R_g \rangle$, of coarse-grained (CG) and atomistic (AA) PCL with chain lengths n = 10-60, at different acetone molar fractions, x_A. The LJ interaction levels are II (ε = 4.5 kJ/mol) for the intrachain interaction P_2-P_2, III (ε = 4.0 kJ/mol) for C_α-C_α and IV (ε = 3.5 kJ/mol) for P_2-C_α. Atomistic results for PCL-40 and PCL-60 are missing in the reference work, as well as all the simulations at x_A =0.25, because of the de-mixing that affected the acetone/water mixture.

PCL-n	**x_A**	**0**		**0.25**		**0.50**		**0.75**		**1.00**	
		AA	CG	AA	CG	AA	CG	AA	CG	AA	CG
n = 10	$\langle R_g \rangle$, nm	0.64	0.68	-	1.00	1.19	1.39	1.23	1.47	1.25	1.48
n = 20	$\langle R_g \rangle$, nm	0.77	0.81	-	1.02	1.66	1.51	1.73	1.75	1.85	2.10

n = 30	$\langle R_g \rangle$, nm	0.88	0.89	-	1.05	2.00	1.58	2.17	1.75	2.42	2.70
n = 40	$\langle R_g \rangle$, nm	-	0.99	-	1.18	-	1.60	-	1.84	-	3.10
n = 60	$\langle R_g \rangle$, nm	-	1.13	-	1.28	-	1.80	-	2.10	-	4.09

The behaviour observed at x_A= 0.50 and, in general, the whole trend reported in Table 3, deserves further comments. The most important one is about what happens at x_A= 0.50. At this acetone molar fraction, the largest gap with atomistic results is detected. Moreover, the trend observed with the CG model shows a sharper globule-to-coil transition, going through intermediate acetone molar fractions, with respect to the atomistic results. This globule-to-coil transition, going from pure "bad" to pure "good" solvent, is clearly shown to be more gradual at the atomistic level, leading to a more stretched conformation already at intermediate acetone molar fractions (x_A = 0.50).

Recent works have shown that the sudden globule-to-coil transition observed here at intermediate molar fraction is a main feature of other CG models of polymer chains in binary mixtures. More specifically, Cheng et al[66] demonstrated that a stepwise transition from globule-to-coil configuration is detected at medium acetone molar fraction in binary mixtures ($x_A \approx 0.55$) for a single polymer tethered chain in solution, in a DPD-based analysis. They also detected that the stepwise transition observed for a single CG chain becomes less sharp for polymer brushes. Raman et al[64] observed the same behaviour at x_A= 0.50 for single CG PCL chains in acetone-water mixtures, by using the MARTINI force filed with a polarizable water model. However, in the results presented here it is not possible to detect a proper stepwise transition[67], despite the CG profile turns out to be much steeper than the atomistic one.

It is also worth pointing out that the atomistic simulation[51] results might be affected by unphysical de-mixing of the solvents mixture since the unmodified OPLS force fields parameters were used in the atomistic results reported in Table 3. The de-mixing was shown to take place at acetone molar fraction equal to 0.25, as a complete phase separation between

the two solvents. This made the simulations unfeasible at that acetone concentration and, for this reason atomistic data at $x_A = 0.25$ are not reported in Table 3.

A possible explanation of the conformational mismatch found out here between atomistic and CG results at $x_A = 0.50$ might be related to an eventual slight de-mixing/clustering still occurring at higher acetone molar fractions than the one pointed out ($x_A = 0.25$) in Di Pasquale et al.[51] Due to the lack of experimental data it is however under debate the uncertainty related to the other atomistic simulations related to acetone molar fractions of 0.50 and 0.75. Furthermore, since this unphysical de-mixing affects the only atomistic simulations in a very narrow range of acetone molar fraction in mixture (around 0.25) and, being the CG simulations not affected by any de-mixing phenomena (as shown in section 2), the whole CG model here developed can be considered reliable and overall robust.

By looking at Table 3, it is noteworthy to stress that also for longer polymer chains (PCL-40 and PCL-60) the trend is the same as the one observed at lower molecular weights. A globule-to-coil transition is detected also here in the range of acetone molar fractions, x_A = [0.50, 0.75]. It is furthermore worth noticing also that the trend obtained by the CG model of PCL in acetone-water mixtures follows the Flory law

$$\langle R_g \rangle \propto {M_w}^{\nu} \tag{8}$$

where M_w is the polymer chain molecular weight (readily calculated from the PCL chain length) and ν corresponds to Flory's exponent that is equal to 1/3 in pure anti-solvent (water) and 3/5 in pure good solvent (acetone), in line with Flory's theory. The trend in pure water and pure acetone for all the M_w investigated here (PCL-10 / -60) is depicted in Figure 7. The CG simulation results are reported here with discrete symbols (blue for water and red for acetone) and Flory's theory predictions with dash-dot lines. An arbitrary constant is used to represent the proportionality relation reported in Equation (8). Atomistic results together with the corresponding Flory law extrapolated in Di Pasquale at al[51] are also reported respectively with discrete triangles (yellow in acetone and white in water) and black dashed lines. Atomistic and CG results are in excellent accordance in water and good accordance in acetone, showing a good Flory law scalability, reported with dot-dashed (CG) and dashed (AA[51]) lines in Figure 7. Error bars are also reported. Concerning the intermediate acetone molar fractions, error bars have shown to be in the range found out for pure water and acetone, presented in Figure 7 and omitted in Table 3 for a sake of clarity of the presented results. As it can be seen, the uncertainty related to simulations in acetone-rich environments is much larger than in pure water.

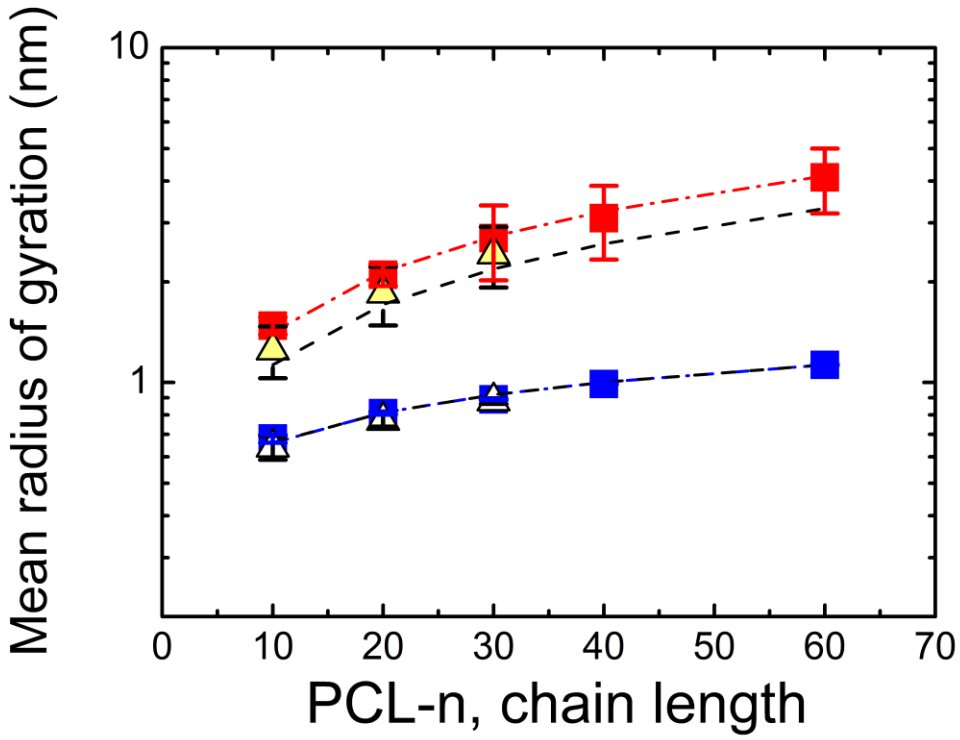

Figure 7. Flory's theory predictions of the CG model developed here in pure good solvent (acetone, red) and pure bad solvent (water, blue) for all the PCL chain lengths investigated in this work. Atomistic results (triangles) and the Flory law extrapolated in the reference work[51] (black dashed lines) are also reported. Error bars are reported. In water and at short polymer chains in acetone, the errors are so small that the error bars collapse on the corresponding symbol.

What is really important to point out from Figure 7 is that in pure solvents the CG model predictions are in an excellent agreement with Flory's theory (red and blue dash-dot lines, corresponding to Equation (8)), namely the mean radius of gyration of the CG model scales with Flory's exponent equal to 1/3 (blue dash-dot line) for bad solvent and to 3/5 (red dash-dot line) for good solvent. The agreement is shown to be slightly better in water, in which also the atomistic agreement was better than in pure acetone.

A last test of the CG model is carried out by simulating multiple PCL-30 chains in pure solvents, at the operating conditions reported in subsection 5.2. As it can be seen in Figure 8, no self-assembly takes place in pure acetone after 50 ns (top panel), whereas CG PCL chains undergo self-assembly in pure water (bottom panel) under the same operating conditions. This result is in line with the physics of the problem here investigated and paves

the way for future investigations of longer (eg, industrial polymer molecular weights) PCL chains in solution.

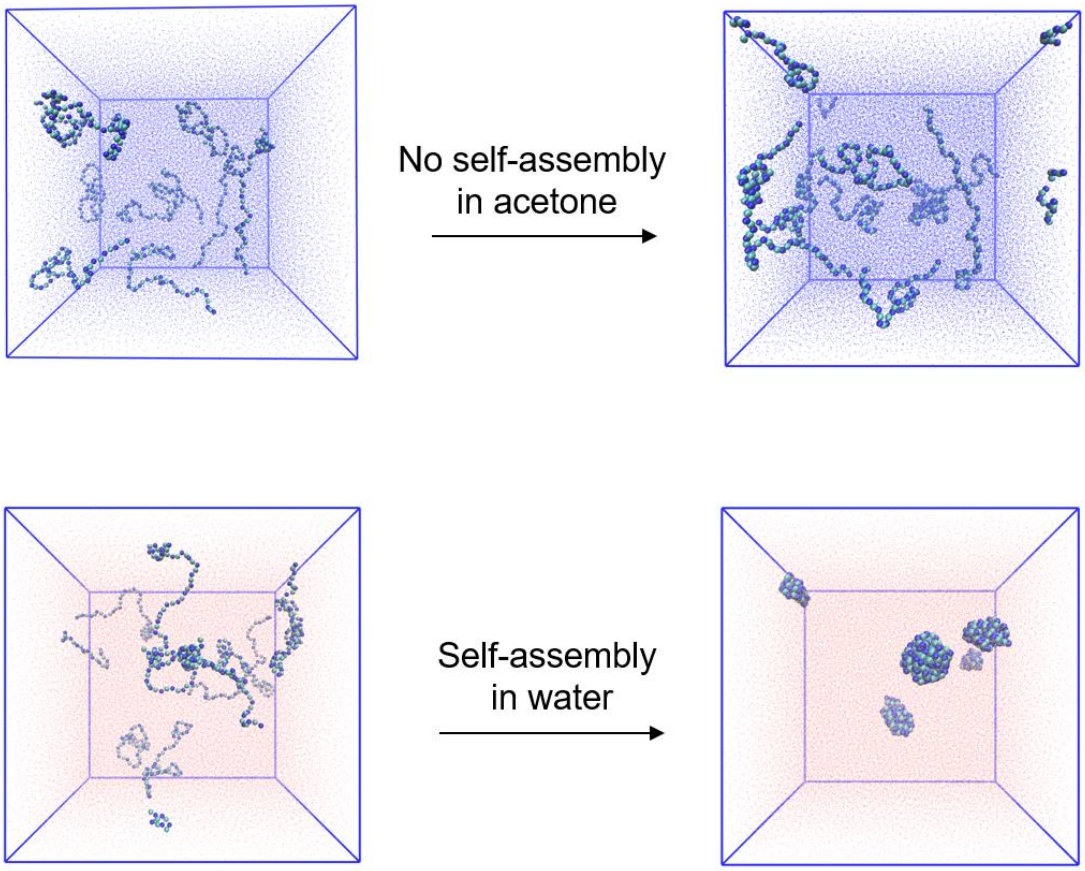

Figure 8. Multiple CG PCL chains in pure solvents. No self-assembly takes place in pure acetone (top); self-assembly takes place in pure water (bottom), as physically expected.

7 CONCLUSIONS

In this work a multiscale molecular dynamics approach for polymer self-assembly in solution is proposed, in which classical all-atom molecular dynamics (MD) is combined with coarse-grained molecular dynamics (CGMD). The model developed here is based on the MARTINI force field[31] and aims to build up a CG model for the poly-ε-caprolactone (PCL) in acetone, water and their mixtures. The adopted strategy consists in optimising both polymer - solvent and intrachain polymer - polymer non-bonded interactions, by following a hybrid thermodynamic/conformational procedure. Concerning the thermodynamics, the solvation free energy of single polymer beads was evaluated by means of the Bennett's Acceptance Ratio (BAR) method.[50] Regarding the conformation of the polymer chains, the mean radius

of gyration was chosen as target property, whose atomistic data are taken from a previous work.[51] Three different PCL chain lengths have been employed in this optimization procedure, that are PCL-10, -20 and -30 (ie, 10, 20 and 30 repeat units). The model optimised on these three chain lengths was also tested for higher molecular weights (PCL-40 and -60). Atomistic simulations related to the solvation free energy were carried out here, by means of different acetone charge distributions, in order to avoid the very well-known issue of the de-mixing of acetone-water mixtures.[52,55]

The thermodynamic procedure showed that a higher degree of polarity (with respect to the standard MARTINI force field) of the bead types that map the polymer in solution must be chosen, in order to correctly reproduce the free energy of solvation.

The conformational results also depict an interesting scenario. First of all, it is a sake of trade-off in finding the best set of intrachain non-bonded LJ parameters, since effects due to the chain length are important especially for single short CG chain lengths. The agreement with atomistic results is very good in pure solvents and, more generally, far away from medium acetone molar fraction. At this threshold acetone concentration in mixture, a sharper globule-to-coil transition is detected for the single PCL chain in solution, with respect to the atomistic profile. This trend was also observed in previous CG simulations of polymer in binary mixtures[64,66] but does not agree with our previous atomistic simulations results where however the model could still suffer from the unphysical de-mixing. Being the latter still related to a very narrow acetone molar fraction range and, since such a phenomenon has been shown here to not take place at the CG level, the developed CG model can be considered robust and consistent with the proposed procedure. Future investigations on the atomistic system can be carried out, in order to find out a clear explanation, since the results pointed out here open to new interesting challenges and under debate analyses.

Investigations of higher PCL molecular weights show the same trend observed for smaller chains, with the same limitations and advantages. The CG model shows to be able to reproduce Flory's scaling predictions in both pure good and bad solvents (for which Flory's exponent is known a priori) and self-assembly takes place in pure water but not in pure acetone, in line with the physical expectations.

PRESENT ADDRESS

§Department of Chemical Engineering, Imperial College London, South Kensington Campus, London SW7 2AZ, UK. Current E-mail: *a.lavino@imperial.ac.uk*

ACKNOWLEDGMENTS

Computational resources were provided by HPC@POLITO, a project of Academic Computing within the Department of Control and Computer Engineering at the Politecnico di Torino (http://www.hpc.polito.it).

DISCLOSURE STATEMENT

No potential conflict of interest was reported by the authors.

REFERENCES

[1] P. Li, K. Merz, *Chem. Rev.* **2017**, *117*, 1564.

[2] M. S. Daw, S. M. Foiles, M. I. Baskes, *Mater. Sci. Rep.* **1993**, *9*, 251.

[3] S. Nawaz, P. Carbone, *J. Phys. Chem. B* **2011**, *115*, 12019−12027.

[4] S. Nawaz, M. Redhead, G. Mantovani, C. Alexander, C. Bosquillon, P. Carbone, *Soft Matter* **2012**, *8*, 6744−6754.

[5] L. Boggioni, I. Tritto, M. Ragazzi, P. Carbone, D. R. Ferro, *Macromol. Symp.* **2004**, *218*, 39−50.

[6] M. Karplus, J. A. McCammon, *Nat. Struct. Biol.* **2002**, *9*, 646.

[7] J. Barrat, J. Banschnagel, A. Lyulin, *Soft Matter* **2010**, *6*, 3430.

[8] M. P. Allen, D. J. Tildesley, *Computer simulation of liquids*, Oxford Science Publication, Oxford (UK) **1987**.

[9] P. Carbone, C. Avendaño, *WIREs Comput. Mol. Sci.* **2014**, *4*, 62−70.

[10] D. L. Cheung, P. Carbone, *Soft Matter* **2013**, *9*, 6841−6850.

[11] H. A. Karimi-Varzaneh, N. F. A. van der Vegt, F. Müller-Plathe, P. Carbone, *ChemPhysChem.* **2012**, *13*, 3428−3439.

[12] T. Taddese, D. L. Cheung, P. Carbone, *ACS Macro Lett.* **2015**, *4*, 1089−1093.

[13] M. Bonomi, G. T. Heller, C. Camilloni, M. Vendruscolo *Curr. Opin. Struc. Biol.* **2017**, *42*, 106-116.

[14] P. D. Dans, A. Zeida, M. R. Machado, S. Pantano *J. Chem. Theory Comput.* **2010**, *6*, 1711−1725.

[15] S. J. Marrink, A. H. de Vries, A. E. Mark, *J. Phys. Chem B* **2004**, *108*, 750−760.

[16] F. Muller-Plathe, *Chem. Phys. Chem.* **2002**, *3*, 754-769.

[17] A. Lyubartsev, A. Laaksonen, *Phys. Rev. E* **1995**, *52*, 3730.

[18] S. Izvekov, M. Parrinello, C. J. Burnham, G. A. Voth, *J. Chem. Phys.* **2004**, *120*, 10896.

[19] S. Izvekov, G. A. Voth, *J. Chem. Phys.* **2005**, *123*, 134105.

[20] W. G. Noid, J. Chu, G. A. Ayton, V. Krishna, S. Izvekov, G. A. Voth, A. Das, H. C. Andersen, *J. Chem. Phys.* **2008**, *128*, 244114.

[21] E. Brini, E. A. Algaer, P. Ganguly, C. Li, F. Rodríguez-Ropero, N. F. A. van der Vegt, *Soft Matter* **2013**, *9*, 2108-2119.

[22] E. Brini, N. F. A. van der Vegt, *J. Chem. Phys.* **2012**, *137*, 154113.

[23] C. Hijon, P. Espanol, E. Vanden-Eijnden, R. Delgado-Buscalioni, *Faraday Discuss.* **2010**, *144*, 301.

[24] N. Di Pasquale, T. Hudson, M. Icardi, *Phys. Rev. E* **2019**, *99(1)*, 013303.

[25] M. P. Howard, A. Z. Panagiotopoulos, A. Nikoubashman, *Comput. Phys. Commun.* **2018**, *230*, 10-20.

[26] R. D. Groot, P. B. Warren, *J. Chem. Phys.* **1997**, *107*, 4423.

[27] D. Kauzlarić, O. Liba, Y. Hanein, P. Español, A. Greiner, S. Succi, J. G. Korvink, presented at 7th IEEE International Conference on Nano/Micro Engineered and Molecular Systems (NEMS), Kyoto, **2012**.

[28] G. Deichmann, V. Marcon, N. van der Vegt, *J. Chem. Phys.* **2014**, *141*, 224109.

[29] H. Droghetti, I. Pagonabarraga, P. Carbone, P. Asinari, D. Marchisio, *J. Chem. Phys.* **2018**, *149(18)*, 184903.

[30] R. Pasquino, H. Droghetti, P. Carbone, S. Mirzaagha, N. Grizzuti, D. Marchisio, *Soft Matter* **2019**, *15*, 1396-1404.

[31] S. J. Marrink, H. J. Risselada, S. Yefimov, D. P. Tieleman, A. H. de Vries, *J. Phys. Chem. B* **2007**, *111*, 7812-7824.

[32] L. Monticelli, S. K. Kandasamy, X. Periole, R. G. Larson, D. P. Tieleman, S. J. Marrink, *J. Chem. Theory Comput.* **2008**, *4*, 819−834.

[33] C. A. Lopez, A. J. Rzepiela, A. H. de Vries, L. Dijkhuizen, P. H. Hunenberger, S. J. Marrink, *J. Chem. Theory Comput.* **2009**, *5*, 3195−3210.

[34] J. J. Uusitalo, H. I. Ingolfsson, P. Akhshi, D. P. Tieleman, S. J. Marrink, *J. Chem. Theory Comput.* **2015**, *11*, 3932−3945.

[35] D. Bochicchio, G. M. Pavan, *ACS Nano* **2017**, *11*, 1000-1011.

[36] G. Rossi, L. Monticelli, S. R. Puisto, I. Vattulainen, T. Ala-Nissila, *Soft Matter* **2011**, *7*, 698–708.

[37] H. Lee, A. H. de Vries, S. J. Marrink, R. W. Pastor, *J. Phys. Chem. B* **2009**, *113(40)*, 13186−13194.

[38] H. Lee, R. G. Larson. *J. Phys. Chem. B* **2006**, *110*, 18204–18211.

[39] T. Taddese, P. Carbone, *J. Phys. Chem. B* **2017**, *121*, 1601-1609.

[40] A. Milani, M. Casalegno, C. Castiglioni, G. Raos, *Macromol Theor Sim* **2011**, *20*, 305–319.

[41] T. Zelenková, M. J. Mora, A. A. Barresi, G. E. Granero, D. Fissore, *J. Pharm. Sci.* **2018**, *107*, 1157-1166.

[42] I. Valente, E. Celasco, D. Marchisio, A. A. Barresi, *Chem. Eng. Sci.* **2012**, *77*, 217-227.

[43] A. Ancona, B. Dumontel, N. Garino, B. Demarco, D. Chatzitheodoridou, W. Fazzini, H. Engelke, V. Cauda. *Nanomaterials* **2018**, *8*, 143.

[44] A. D. Lavino, N. Di Pasquale, P. Carbone, D. Marchisio, *Chem. Eng. Sci.* **2017**, *171*, 485-494.

[45] C. Wu, T. Jim, Z. Gan, Y. Zhao, S. Wang, *Polymer* **2000**, *41*, 3593−3597.

[46] L. S. Jabr-Milane, L. E. van Vlerken, S. Yadav, M. M. Amiji, *Cancer Treat. Rev.* **2008**, *34*, 592−602.

[47] T. K. Dash, B. Konkimalla, *Mol. Pharmaceutics* **2012**, *9*, 2365−2379.

[48] H. Maeda, G. Y. Bharate, J. Daruwalla, *Eur. J. Pharm. Biopharm.* **2009**, *71*, 409−419.

[49] A. D. Lavino, D. Marchisio, M. Vanni, A. Ferri, A. A. Barresi, *Chem. Today* **2019**, *37(4)*, 8-11.

[50] C. H. Bennett, *J. Comp. Phys.* **1976**, *22*, 245–268.

[51] N. Di Pasquale, D. L. Marchisio, A. A. Barresi, P. Carbone, *J. Phys. Chem. B* **2014,** *118*, 13258–13267.

[52] R. G. Pereyra, M. L. Asar, M. A. Carignano. *Chem. Phys. Lett.* **2011**, *507*, 240-243.

[53] A. Perera, F. Sokolic, *J. Chem. Phys.* **2004**, *121*, 11272.

[54] J. N. Israelachvili, *Intermolecular and Surface Forces*, 3rd ed., Academic Press, San Diego **2011**.

[55] A. D. Lavino, L. Banetta, P. Carbone, D. Marchisio, *J. Phys. Chem. B* **2018**, *122*, 5234−5241.

[56] M. R. Shirts, V. S. Pande *J. Chem. Phys.* **2005**, *122(14)*, 144107.

[57] S. Bruckner, S. Boresch, *J. Comp. Chem.* **2011**, *32(7)*, 1303-1319.

[58] R. F. Cross, P. T. McTigue, *Aust. J. Chem.* **1977**, *30*, 2597-2612.

[59] R. E. Skyner, J. L. McDonagh, C. R. Groom, T. van Mourika, J. B. O. Mitchell, *Phys. Chem. Chem. Phys.* **2015**, *17*, 6174.

[60] E. M. Duffy, W. L. Jorgensen, *J. Am. Chem. Soc.* **2000**, *122*, 2878-2888.

[61] D. Wu, D. A. Kofke, *J. Chem. Phys.* **2005**, *123*, 084109.

[62] B. Hess, C. Kutzner, D. van der Spoel, E. Lindahl, *J. Chem. Theory Comput.* **2008**, *4*, 435−447.

[63] T. Beutler, A. Mark, R. van Schaik, P. Gerber, W. van Gunsteren, *Chem. Phys. Lett.* **1994**, *222*, 529-539.

[64] A. S. Raman, A. Vishnyakov, Y. C. Chiew, *Mol. Simulat.* **2017**, *43*, 92-101.

[65] A. Ben-Naim, Y. Marcus, *J. Chem. Phys.* **1984**, *81*, 2016.

[66] J. Cheng, A. Vishnyakov, A. V. Neimark, *Langmuir* **2014**, *30*, 12932−12940.

[67] S. Sun, I. Nishio, G. Swislow, T. Tanaka, *J. Chem. Phys.* **1980**, *73*, 5971-5975.

FIGURE CAPTIONS

Figure 1. From left to right there are reported the three snapshots related to acetone molar fractions equal to 0.25, 0.50 and 0.75 respectively in cubic simulation boxes of 3 nm length. It is clear how no de-mixing occurs.

Figure 2. Atomistic radial distribution functions for acetone-acetone, $g_{AA}(r)$, water-acetone, $g_{WA}(r)$ and water-water, $g_{WW}(r)$, at different acetone molar fractions, x_A. The red, green and black lines correspond respectively to x_A= 0.25, 0.50 and 0.75.

Figure 3. Initial mapping of both the PCL chain and the solvents used in this work. The repeat unit is described by N_{am} and C_1 bead types respectively for the ester and the alkyl part. These choices represent just a starting point for the optimization procedure in building up the CG model. Water and acetone are instead mapped respectively by P_4 and N_a bead types.

Figure 4. (a) Snapshot of the N_a-P_4 CG acetone(blue)-water(pink) mixture for x_A = 0.25 and box length equal to 15 nm, with 27000 particles and after 10 ns. (b) Detail of the N_a-P_4 box in which a little cluster (blue, N_a) it seems to form; however, no evident phase separation is detected at the CG level. Densities profiles along x (black), y (red) and z (green) are reported at acetone molar fraction equal to 0.25 (c), 0.50 (d) and 0.75 (e).

Figure 5. Free energy of solvation of butane (squares) and methyl formate (triangles) in mixture from the atomistic simulations (black symbols) carried out in this work. The red symbols refer to the MARTINI model, C_1 (squares) and N_{am} (triangles), without any modifications of the LJ parameter, ε. The purple symbols refer to the CG model developed here, in terms of single beads (squares for the alkyl part and triangles for the ester part of the PCL repeat unit) varying suitably the LJ parameter, ε. The green symbols stand for the experimental ΔG^{solv} values respectively of butane and methyl formate in pure water.

Figure 6. Snapshots referred to the final configuration of the CG PCL, after the optimization procedure conducted on the atomistic radius of gyration. The LJ interaction levels are: II (ε = 4.5 kJ/mol) for the intrachain interaction P_2- P_2, III (ε = 4.0 kJ/mol) for C_α- C_α and IV (ε = 3.5 kJ/mol) for P_2- C_α. This scheme refers to the numerical results reported in Table 3.

Figure 7. Flory's theory predictions of the CG model developed here in pure good solvent (acetone, red) and pure bad solvent (water, blue) for all the PCL chain lengths investigated in this work. Atomistic results (triangles) and the Flory law extrapolated in the reference work[45] (black dashed lines) are also reported. Error bars are reported. In water and at short polymer chains in acetone, the errors are so small that the error bars collapse on the corresponding symbol.

Figure 8. Multiple CG PCL chains in pure solvents. No self-assembly takes place in pure acetone (top); self-assembly takes place in pure water (bottom), as physically expected.

TABLES CAPTIONS

Table 1. Acetone charge (e) distribution used at different acetone molar fractions, x_A. C2-O2 corresponds to the carbonyl group; all the other atoms correspond to the two methyl groups. For each charge distribution, the corresponding acetone dipole moment is reported.

Table 2. Lennard-Jones interactions MARTINI type and corresponding ε parameter value, between the repeat unit bead types P_2, C_α and the solvent bead types P_4 and N_a.

Table 3. Mean radius of gyration, $\langle R_g \rangle$, of coarse-grained (CG) and atomistic (AA) PCL with chain lengths n = 10-60, at different acetone molar fractions, x_A. The LJ interaction levels are II (ε = 4.5 kJ/mol) for the intrachain interaction P_2-P_2, III (ε = 4.0 kJ/mol) for C_α-C_α and IV (ε = 3.5 kJ/mol) for P_2-C_α. Atomistic results for PCL-40 and PCL-60 are missing in the reference work, as well as all the simulations at x_A =0.25, because of the de-mixing that affected the acetone/water mixture.